Continental scale vegetation index from Indian geostationary satellite: algorithm definition and validation

Rahul Nigam[1,*], Bimal K. Bhattacharya[1], Keshav R. Gunjal[1], N. Padmanabhan[2] and N. K. Patel[1]

[1]Agriculture-Forestry and Environment Group, Space Applications Centre (ISRO), Ahmedabad 380 015, India
[2]Data Products Software Group, Space Applications Centre (ISRO), Ahmedabad 380 015, India

Time series vegetation index using observations of the earth from space platform is a valuable source to derive several plant biophysical parameters for ecological, hydrological, climate models and to study land-use land-cover change dynamics. Indian geostationary satellite (INSAT 3A) sensor (CCD) observes the earth surface with continental (Asia) coverage at 1 km × 1 km spatial resolution and high temporal frequency (half-an-hour) at constant view direction. This study was aimed at defining and implementing an algorithm to retrieve normalized difference vegetation index (NDVI) at continental scale from INSAT 3A CCD surface reflectances in red (0.62–0.68 μm), near infrared (0.77–0.86 μm) bands and evaluate it with the global product. The methodology includes vicarious calibration, cloud screening, atmospheric correction of at-sensor reflectances and development of protocol. The temporal dynamics of 16-day NDVI composite at 0500 GMT (10 : 30 local mean time) for a growing year (June 2008–April 2009) showed matching profiles with respect to global products (e.g. MODIS TERRA) over known land targets such as agriculture, forest and desert. The root mean square deviation between the two was 0.13 with correlation coefficient (*r*) 0.83. The differences were attributed to surface anisotropy, view angle difference and differences in spectral bandwidths with their relative positions in the electromagnetic spectrum.

Keywords: Asia, CCD, geostationary, INSAT, normalized difference vegetation index.

THE normalized difference vegetation index (NDVI) is defined as the ratio of difference and sum of surface reflectances in near infrared (NIR) and red bands. It is an indicator of the amount of green biomass[1]. It has a strong theoretical basis as a measure of the solar photosynthetic active radiation (PAR) absorbed by the canopy[2]. NDVI relates reflectance (or radiance) in the red and NIR bands to plant biophysical variables such as leaf area index (LAI), canopy cover and the concentration of the leaf chlorophyll. For land surfaces dominated by vegetation, the practical range of NDVI is from 0.1 to 0.9 during a growing season, the higher values being associated with greater density and greenness of the plant canopy. Atmospheric effects, such as molecular scattering, aerosol scattering, gaseous absorption by atmospheric constituents (ozone, water vapour) and clouds, all tend to increase the value of red reflectances with respect to NIR when observed from space platform, thus reducing NDVI.

The quantitative estimation of most of the biophysical parameters using satellite-based optical remote sensing requires time series NDVI data as input[3,4]. Daily and time composite NDVI series from moderate (≤ 1 km) to coarse (> 1 km) resolution sensor data can provide 'full resolution' of vegetation growth cycle than a single date high-resolution optical data with low repeativity[5,6]. Time series NDVI are extremely useful (i) to derive phenological metrics[7], (ii) to evaluate land-use land-cover change[8], (iii) to monitor in-season vegetation conditions anomaly through inter-annual comparison[9] and (iv) to quantify LAI/fractional absorbed PAR[10] and ecosystem productivity[11]. This is also an important land surface input to climate models. The time series NDVI product is now-a-days regularly available from observations in red and NIR bands from wide-view global polar orbiting sensors such as: SPOT-VGT, MODIS TERRA and AQUA, NOAA AVHRR at spatial resolutions varying between 250 m and 8 km.

These are available maximum twice per day on daily or time composite basis. The NDVI generated at multiple times in a day from geostationary satellite sensors provide opportunity to get more clear-sky NDVI as compared to 1–2 overpasses in a day by polar orbiting wide view sensor[12]. The effects due to orbital drift in polar orbiting sensors are absent in case of geostationary sensors which have constant viewing geometry with respect to earth targets. Moreover, the diurnal behaviour of narrow band surface reflectances in response to solar zenith and azimuth angles with fixed sensor viewing geometry is ideal to characterize surface bi-directional reflectance distribution function (BRDF) of different land targets.

*For correspondence. (e-mail: rahulnigam@sac.isro.gov.in)

Geostationary sensor has a continental scale coverage from a single snapshot. Therefore, it has less turn-around-time (TAT) from acquisition to generation of a continental scale NDVI product. In contrast, tile-by-tile processing is required to produce continental scale NDVI mosaic from wide view polar orbiting sensor thereby increasing the TAT. Even the spatial consistency of continental NDVI mosaic gets diluted due to intermittent loss of data in different tiles at different times. But spatial consistency in observations is maintained for a given assured coverage over a continent from geostationary sensors. No other existing geostationary satellite missions in the world except INSAT 3A CCD (1 km spatial resolution) of India and MSG SEVIRI (3 km spatial resolution) have payloads that take multiple observations per day in multi-spectral optical bands. INSAT 3A is the only geostationary satellite which scans Asia with multi-spectral bands.

INSAT 3A was launched in 2005 with sub-satellite longitude at 93.5°E. It covers one-fourth of the globe in a single snapshot mainly the Asia continent (44.5°E to 105.3°E, 9.8°S to 45.5°N). It has CCD payload that was specifically designed to monitor vegetation and snow cover conditions over Asia regularly at spatial resolution of 1 km × 1 km. It has three unique optical bands in red (0.62–0.68 μm) also called visible, NIR (0.77–0.86 μm), short-wave infrared (SWIR) (1.55–1.69 μm) wavelength regions. Thus, it acts as a complementary sensor to high resolution polar orbiting IRS P6 AWiFS sensor (56 m spatial resolution) which is meant to pinpoint the detailed local scale study with similar bands if indicated through quick assessment by CCD at continental scale. The co-registered and georegistered ASIA mercator products at uniform pixel size in TM projection in three bands are generated within 10 min of image acquisition after basic corrections for servo, ephimeris extraction, stagger correction and template registration through INSAT Meteorological Data Processing System (IMDPS) operational software. The present study was undertaken (i) to define and implement atmospherically corrected algorithm for vegetation index (NDVI) at continental scale for geostationary satellite and (ii) to validate the operational continental CCD NDVI products with global available product.

Methodology

The reflected radiances from earth surface reaching satellite sensors are generally influenced by sun-sensor viewing geometry and atmospheric noises, adjacency and BRDF effects. Corrections are needed to remove these effects to convert spectral reflectances (R_i) at sensor into surface spectral reflectances. These corrections are categorized as follows.

Level 1: Generation of angular normalized atmospherically corrected surface spectral reflectances.

Level 2: Level 1 + adjacency effect correction.

Level 3: Level 2 + BRDF correction.

Level 1: correction has three different components.

A. Molecular scattering

B. Gaseous absorption (ozone, water vapour, CO_2)

C. Aerosol scattering and absorption.

Post launch vicarious calibration of band reflectances

It has been found from earlier analysis that NDVI computed with pre-launch calibration coefficients for red and NIR bands showed significant non-linear bias that increased with increase in NDVI values[13]. Further studies also found that NIR top-of atmosphere (TOA) band at-sensor radiances become saturated at higher radiances when pre-launch calibration is used. This indicated that performance of CCD sensor elements degraded due to space weathering[14,15]. INSAT 3A CCD does not have on-board calibration mechanism. Direct calibration with *in situ* measurements is also not feasible at such coarser spatial resolution (1 km) due to lack of homogeneous patch and spatial representativeness of *in situ* measurements. Therefore, a vicarious post-launch calibration has been carried out by cross-calibrating, coregistered and calibrated TOA radiances in red and NIR bands of similar spectral widths from high resolution (56 m) IRS-P6 AWiFS sensor under equal atmospheric influences. Three clear sky dates spread over December, February and March for both INSAT 3A CCD and AWiFS having same overpass time (0500 GMT) were chosen for cross-calibration. TOA band radiances from six different land categories such as agriculture, forest, snow, bare soil, water body and cloud were used for recalibration. The linear calibration curves were developed between AWiFS and INSAT 3A CCD TOA band radiances with fairly high correlation for red ($y = 1.83x - 5.8$, $R^2 = 0.96$) and NIR ($y = 1.58x - 4.94$, $R^2 = 0.92$) bands. The improvement in radiance can thus be achieved through recalibration[16]. In vicarious calibration studies, the nominal on-orbit radiometric calibrations of many satellite sensors have been found to fit within their predicted uncertainties[17].

Atmospheric corrections

The cloud screening and atmospheric correction were applied on the cross-calibrated TOA reflectances. These were computed as

$$\rho_{\mathrm{TOA}(\lambda)} = \frac{\pi d^2 L_{\mathrm{TOA}(\lambda)}}{E_{0(\lambda)} \cos\theta_s}, \quad (1)$$

where $L_{\mathrm{TOA}(\lambda)}$ is the at-sensor cross-calibrated band radiances in $\mathrm{Wm^{-2}\,\mu m^{-1}\,sr^{-1}}$ in a given band of CCD, d the Earth–Sun distance correction factor and calculated as follows[18]

$d = (1 - 0.01672 \times \cos(0.9856 \times (\text{C. day} - 4)))$.

$E_{0(\lambda)}$ is the exo-atmospheric bandpass irrradiances weighted through CCD relative spectral response (RSR) at fixed wavelength interval[19], C. day, the Calendar day and θ_s the solar zenith angle (degree). The CCD sensor characteristics are summarized in Table 1.

The optical properties of cloud showed that its TOA reflectances in red, NIR or cloud albedo in broad visible band become high and even more than 90%. But SWIR band reflectances are less in presence of water clouds due to higher absorption. Three criteria were fixed for different cloud types such as cirrus (high level), alto (medium level) and cumulus (low level) clouds based on several CCD scenes. The first two criteria were only based on TOA reflectance thresholds in red and NIR bands due to presence of more of ice clouds. In the third criterion, SWIR TOA reflectance threshold was introduced in addition to red and NIR reflectances due to increasing presence of water clouds. Further processing was carried out only in cloudfree pixels.

TOA reflectances in cloudfree pixels were corrected for atmospheric noises such as molecular and aerosol scattering along with gaseous absorption using simple model for atmospheric corrections (SMAC) with default coefficients[20]. This has been successfully used for wide view satellite sensors such as NOAA AVHRR, METEOSAT, etc.

The generalized functional form of SMAC model is

$$\rho^*(\theta_s, \theta_v, \Delta\phi) = t_g(\theta_s, \theta_v)\{\rho_a(\theta_s, \theta_v, \Delta\phi) + T(\theta_s)T(\theta_v)\rho_c/(1 - \rho_c S)\}, \quad (2)$$

with

$$T(\theta) = e^{-\tau/\mu} + td(\theta), \quad (3)$$

where $\theta = \theta_s$ or θ_v, ρ^* is the TOA spectral reflectance at satellite sensor level, ρ_c the spectral surface reflectance, θ_s the sun zenith angle, θ_v the view zenith angle, $\Delta\phi$ the relative azimuth between sun and sensor, t_g the total gaseous transmission, ρ_a the atmospheric reflectance which depends on optical properties of air molecule, aerosol, and sun-sensor viewing geometry, τ the atmospheric optical depth with e^{τ/μ_s} and e^{τ/μ_v}, being the direct atmospheric transmission in sun (θ_s) and view (θ_v) direction, $td(\theta)$ atmospheric diffuse transmittance, S the spherical albedo of the atmosphere.

The term, $(1 - \rho_c S)$, is considered to take into account of multiple scattering between surface and the atmosphere.

This atmospheric correction scheme includes first-order correction for additive and multiplicative atmospheric perturbations. This assumes lambertian surface and is simple to implement, calibrated and tested against 5S atmospheric radiative transfer code thus increasingly being used for generating surface reflectances from TOA reflectances. Apart from sun-sensor angular geometry, this requires atmospheric inputs such as columnar ozone, precipitable water and aerosol optical depth (AOD) at 0.55 μm. The database on daytime mean of five years' (2002–2006) ozone, precipitable water and aerosol optical depth at 0.55 μm from MODIS TERRA (0530 GMT) and AQUA (0800 GMT) was prepared through interpolation of MODIS eight-day atmospheric products ($1° \times 1°$) down to CCD resolution. The overall flow of NDVI retrieval from CCD is shown in Figure 1.

Validation strategy

To evaluate the performance of atmospherically corrected CCD NDVI, it has been first compared with non-atmospherically corrected CCD NDVI for a day. The three day corrected and uncorrected CCD NDVI on three days representing different seasons of a growing year were compared between May 2008 and April 2009 with MODIS TERRA NDVI for known natural targets. Again 16-day CCD NDVI composites were compared with global available MODIS TERRA NDVI for different land cover types throughout the year. Direct validation of such a coarse NDVI with *in situ* point measurements is not feasible. In the present study, MODIS TERRA (MOD13Q1) (at 0500 GMT) NDVI tiled product (4800×4800) at 250 m were used as reference for comparison

Table 1. Characteristics of INSAT 3A CCD, AWiFS and MODIS TERRA

Sensor characteristics	INSAT 3A CCD	AWiFS	MODIS TERRA
Number of spectral bands	3	4	36
Bandwidth for Green	–	0.52–0.59 μm	0.54–0.56 μm (band 4)
RED	0.62–0.68 μm	0.62–0.68 μm	0.62–0.67 μm (band 1)
NIR	0.77-0.86 μm	0.77–0.86 μm	0.84–0.87 μm (band 2)
SWIR	1.55–1.69 μm	1.55–1.70 μm	1.62–1.65 μm (band 6)
Spatial resolutions	1000 m (RED, NIR, SWIR)	56 m (GREEN, RED, NIR, SWIR)	250 m (bands 1–2) 500 m (bands 3–7) 1000 m (bands 8–36)
Radiometric resolution	10 bit	10 bit	12 bit

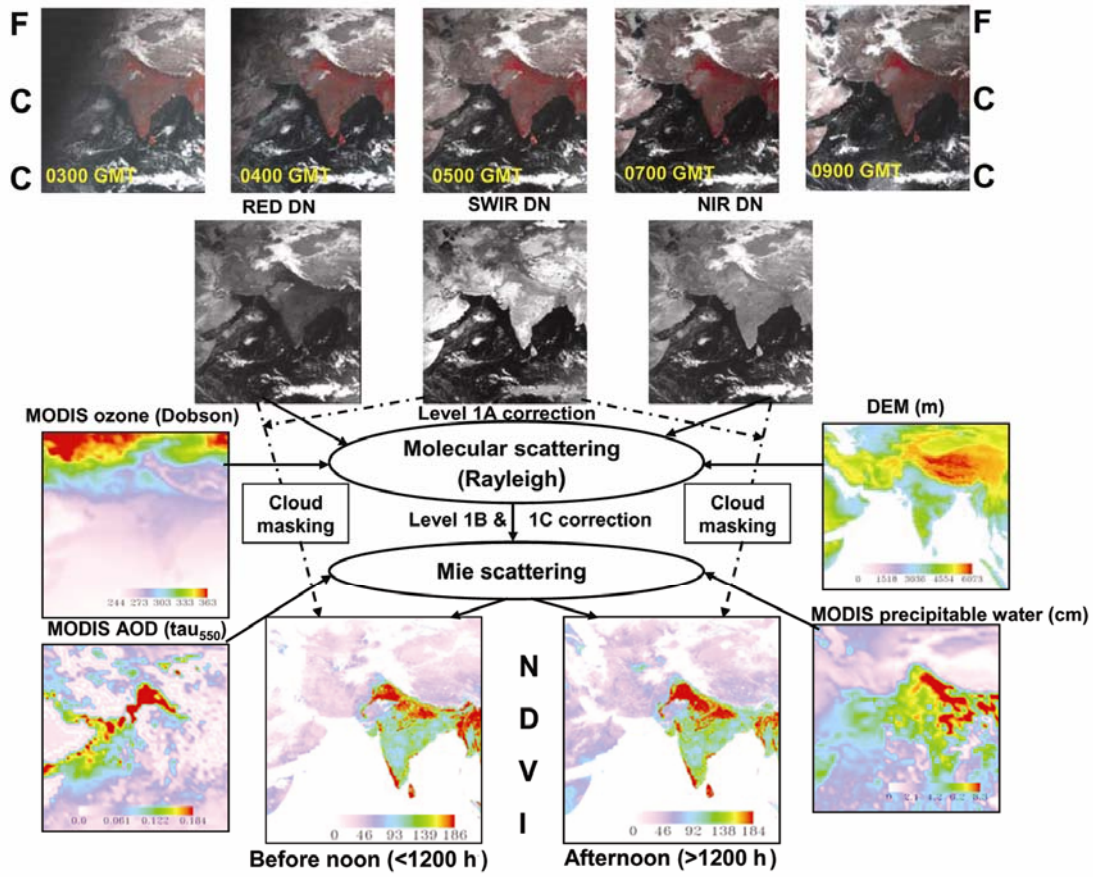

Figure 1. Flow diagram of retrieval of scaled (integer) NDVI from INSAT 3A CCD (7 February 2008; FCC means false colour composites).

with CCD NDVI. A linear aggregation of MODIS TERRA NDVI from 250 m was applied to scale it up to target CCD resolution. The composites were used to minimize the cloud interference on daily NDVI and to capture the phenological shift. The validation has been done through linear aggregation of MODIS TERRA NDVI from native resolution. In order to minimize the effect of sub-pixel heterogeneity, only known natural targets were chosen for validation purposes.

Results and discussions

Effect of atmospheric correction on CCD NDVI

It was found that on a given day, the NDVI range increased from –0.2 to 0.6 in uncorrected one to –0.2 to 0.7 in atmospherically corrected one. The frequency distribution of uncorrected, corrected NDVI and percentage difference between them are exemplified in Figure 2 *a*, *b* and *c*, respectively. Although difference in NDVI ranged from –25% to 45%, a majority of the pixels showed difference varying between 5% and 37%. More detailed analysis was carried out using the NDVI products spread over different parts of a growing year (June–May). The corrected and uncorrected NDVI of CCD for three dates (10 June, 10 October and 10 December 2008) has been compared with MODIS TERRA NDVI of that day for known land cover types. For agriculture cover type, root mean square deviation (RMSD) of uncorrected CCD NDVI was 0.11 whereas, for corrected one it was 0.06. In forest, RMSD of corrected CCD NDVI was substantially lower (0.09) as compared to (0.17) uncorrected CCD NDVI. In desert, less difference was observed for corrected (RMSD = 0.018) and uncorrected (RMSD = 0.029) CCD NDVI. In all, RMSD of corrected NDVI was 0.06 (22.5% of MODIS TERRA NDVI mean) which was substantially lower than uncorrected ones producing a higher RMSD of 0.12 (46.4% of MODIS TERRA NDVI mean). Difference between corrected and uncorrected CCD NDVI on above stated dates is shown in Figure 3. It is evident that the difference in NDVI varied from –0.1 to 0.2 with negative change mostly restricted to bare to low vegetation conditions (for NDVI 0.1–0.3) such as 10 June which corresponds to starting of a growing year. Positive changes after correction were prominent at moderate to high vegetation (for NDVI 0.3–0.8). Atmospheric correction generally includes both additive (and subtractive)

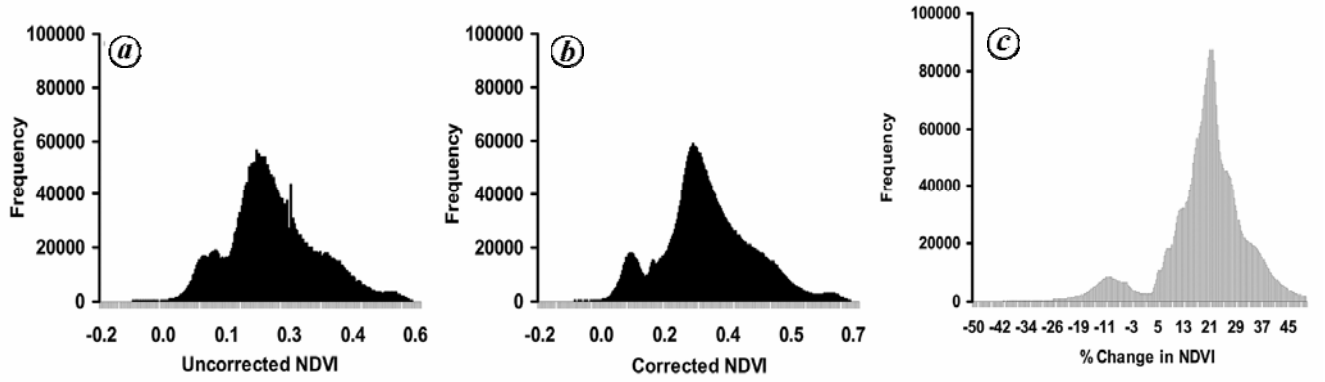

Figure 2. Comparison of histogram of atmospherically corrected and uncorrected NDVI.

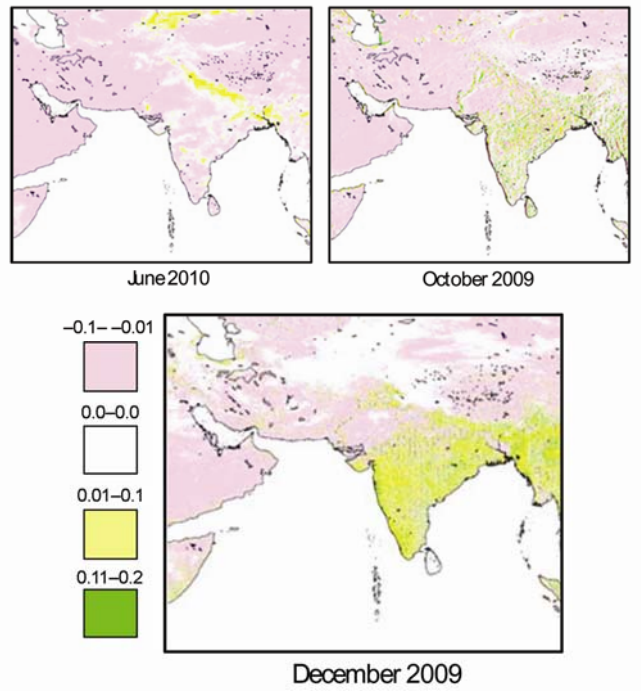

Figure 3. NDVI difference image (atmospheric corrected–uncorrected) on different days in a growing year.

and multiplicative (or divisive) components (eq. (2)). In low vegetation conditions, difference in NIR and red reflectances is very less. The red spectral albedo remains significantly higher (except for dark background either with black soil or wet soil) than the well-vegetated conditions and NIR spectral albedo becomes lower than that of well-vegetated conditions. This leads to increase in red reflectances and decrease in NIR reflectances after correction through non-linear way as in eq. (2). In contrast, well-vegetated system showed increase in NIR reflectance and decrease in red reflectance after atmospheric correction. Therefore, NDVI increases in moderate to well-vegetated system but decreases in low vegetation or bare soil after atmospheric correction. Therefore, it widens the NDVI spatial range after atmospheric correction. The sensitivity of each atmospheric constituent on magnitude of correction for different land cover types has already been summarized by earlier workers[21].

Seasonality test for CCD NDVI

Time series of CCD NDVI composite for a growing year (May 2008–April 2009) was compared with 16-day TERRA NDVI for testing the seasonality. NDVI were extracted over different known land targets such as agriculture, forest and desert. The temporal evolution of CCD NDVI and slope of the profiles match quite well throughout the growing year with TERRA NDVI as presented in Figure 4. Temporal profile over agricultural target in Punjab (30.5°N, 76.4°E) typically showed two peaks corresponding to a sequence of two crops, rice followed by wheat. In case of desert, NDVI from both showed little seasonal variation between 0.05 and 0.2 except small peak during south-west monsoon period. The NDVI profiles from both the sensors showed similar pattern over forest target.

The MODIS NDVI showed higher value in all the three land cover types between 1 and 9 fortnight on *x*-axis as shown in Figure 4 (June–September). After that, INSAT 3A CCD NDVI crosses MODIS and showed higher value (October onwards). This may be due to change in sun-sensor geometry with change in season. This can be explained by seasonal variation in the solar azimuth angle. In June–September, the path of the sun is tending towards north of India, creating a more backward scatter situation (the location of the sensor being fixed on equator at 93.5°E) resulting in lowering of INSAT 3A CCD NDVI values. In October–November, the sun passes south of equator thereby creating a forward scatter situation generally increasing the INSAT NDVI values. Varying solar azimuth angles evidently also influence MODIS data but its effect gets compensated due to varying sensor

azimuth angle. In geostationary satellite, the view remains fixed whereas in polar sensor, the view angle changes with time. The crossing of both NDVI seasonal variation was well marked in a homogenous patch of desert and evergreen forest where surface anisotropy influencing directional reflectance is minimum. In agriculture, two crop growth cycles were evident from both the NDVI curves and surface heterogeneity and anisotropy are generally more than desert and forest. These might cause lesser MODIS NDVI than CCD NDVI when NDVI curves cross each other with reversal trend in the NDVI growth curves as compared to the rest of the year. In MODIS, surface anisotropy was taken into account through BRDF correction while lambertian surface was assumed to compute INSAT 3A CCD NDVI. Similar findings were also reported with MSG SEVIRI sensor when compared with MODIS NDVI[12].

The spikes in the NDVI curve during monsoon months (June–September) could be due to differences in detection methods of cloud contaminated pixels. In MODIS, both optical and thermal bands were used for cloud screening[22]. But only the optical band data were used for cloud screening in CCD. The RMSD of CCD NDVI was 0.13 with a correlation of 0.83 (n = 270) and mean bias of 0.07 with respect to TERRA NDVI. The 1 : 1 validation plot is shown in Figure 5. The statistical analysis (Table 2) showed higher error (0.15) in the NDVI class of 0.2–0.4 that corresponds to less fractional vegetation cover. This could be due to influence of higher surface anisotropy on MODIS NDVI than CCD NDVI at low cover conditions. But the errors were reduced at higher NDVI when surface closer to homogenous or lambertian. The error statistics were also evaluated for different land cover types as shown in Table 3. Among different land cover types, maximum RMSD of 0.14 was noticed in croplands. Agriculture being highly dynamic showing prominent seasonality has more surface anisotropy specially during early growth stage and towards maturity. The dynamics in leaf orientation, leaf angle distribution, canopy geometry at different stages of crop growth are the major causes of higher surface anisotropy. The forest canopies are relatively more homogenous except deciduous canopy thus resulting in less anisotropy and deviation. In desert, the lowest RMSD of 0.04 was noticed because the rate of change of NDVI was very low and the surface appears to be bare except in highly shifting sand dunes thereby indicating the relative homogeneity of bare surface.

In the other available geostationary satellite, METEOSAT second generation (MSG), the SEVIRI cloudfree daily averaged NDVI (3 km) was compared with resampled daily MODIS TERRA/AQUA NDVI (250 m) over a single Dahra site in Africa[12]. They showed fairly good agreement in the dynamic range with a tendency to have little higher MSG NDVI in the beginning of the growing season (July–August) and lower towards

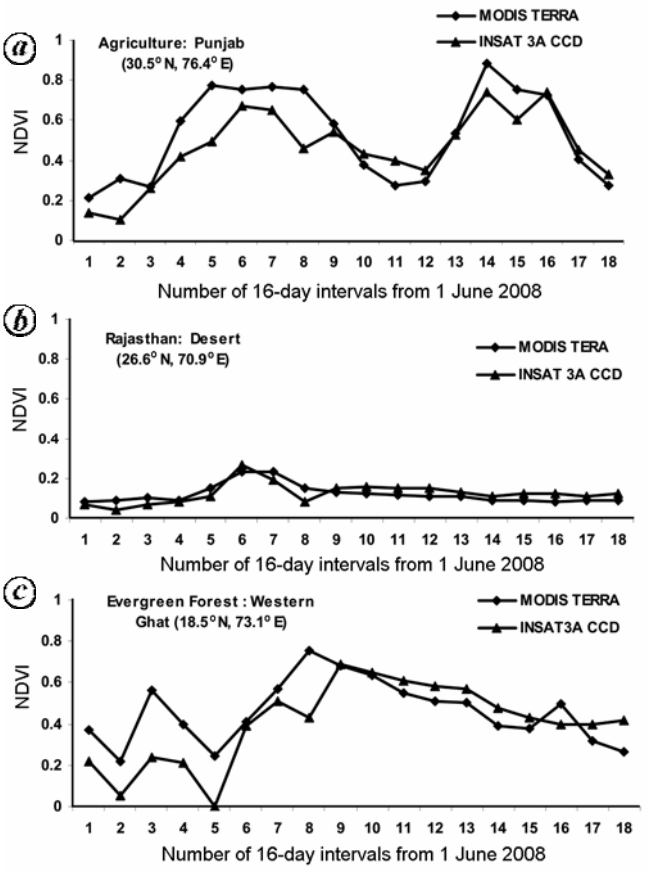

Figure 4. Comparison of temporal profiles of CCD and TERRA NDVI over different land targets.

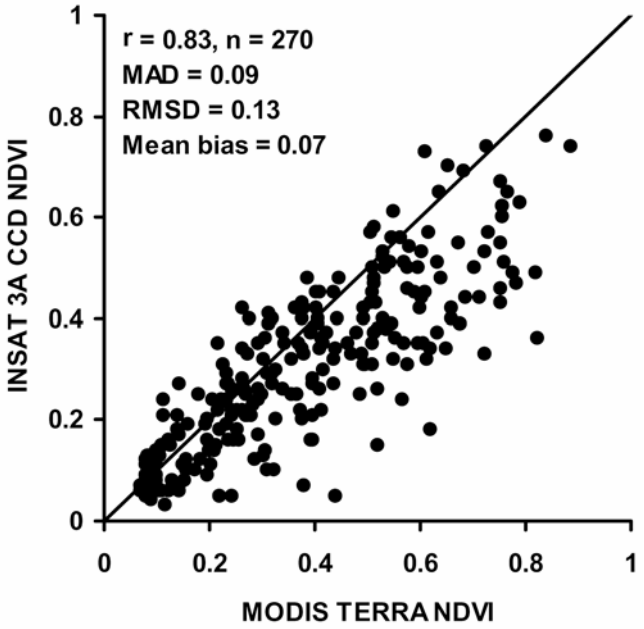

Figure 5. Validation plot of INSAT 3A CCD NDVI with respect to MODIS TERRA NDVI.

Table 2. Error statistics of CCD NDVI at 0500 GMT as compared to MODIS TERRA NDVI at different NDVI classes

CCD NDVI class	*n*	RMSD	MAD
0.0–0.2	94	0.11	0.07
0.2–0.4	105	0.15	0.11
0.4–0.6	59	0.14	0.11
0.6–0.8	12	0.09	0.08

$$\text{RMSD} = \sqrt{\frac{\sum_i [(P_i) - (O_i)]^2}{n}}\ ;\ \text{MAD} = \frac{\sum_i ABS[(P_i) - (O_i)]}{n}$$

where P_i – NDVI_{CCD} at ith case; O_i = $\text{NDVI}_{\text{MODIS}}$ at ith case; n = number of paired datasets.

Table 3. Error statistics of CCD NDVI as compared to MODIS TERRA for different land cover types

Land cover type	*n*	RMSD	MAD
Crop land	144	0.18	0.14
Forest	72	0.14	0.10
Desert	54	0.03	0.03

its end (October–November). Comparison of CCD NDVI with MODIS TERRA in the present study showed good agreement and was at par with earlier findings.

Attempts have already been made to compare available global moderate to coarse resolution NDVI products with ground observations and with other sensors[23]. They compared MODIS, 16-day TERRA and AQUA NDVI with NOAA-16 AVHRR (1 km) 16-day NDVI for different land cover types and observed that MODIS-derived NDVI always showed higher magnitude as compared to AVHRR with a mean bias of 0.05 (ref. 23). The maximum correlation between MODIS and AVHRR was found in evergreen forest. Simulated NDVI for MODIS and AVHRR were also compared and they found slightly higher NDVI from MODIS than those from AVHRR for a variety of plant chlorophyll content levels[24].

It is also reported[25] that higher MODIS NDVI was found as compared to ASTER (90 m) NDVI with mean bias of 0.031 even from the same (TERRA) platform having identical sun-sensor-target geometry. In general, MODIS bands are much narrower in spectral bandwidths than ASTER red and NIR bands. Likewise, the central wavelengths from two sensors differ. MODIS red band completely avoids the red edge region (~ 680 nm), the ASTER counterpart extends to cover that wavelength. These are the consequences of the MODIS band selection requirements to avoid Fraunhofer lines and atmospheric absorption lines. Similarly, MODIS TERRA NDVI showed in general higher NDVI with mean bias ($\text{NDVI}_{\text{MODIS}}$ – NDVI_{CCD}) of 0.07 as compared to CCD NDVI with differing sensor viewing conditions and spectral bandwidths. In addition, present CCD NDVI algorithm does not explicitly consider complex modelling of surface BRDF and adjacency effects as incorporated in MODIS-based algorithm.

Sources of uncertainties

The sensors on different satellite instruments that observe in red and NIR bands showed differences in spectral bandwidths. Systematic differences occurred because the bands receive slightly different components of the reflectance spectra of surface[26]. The CCD sensor has different spectral, spatial and radiometric resolutions as compared to MODIS TERRA. The NDVI computed from CCD spectral bands have bandwidths quite different from MODIS. The bandwidths of MODIS red and NIR are narrow (50 and 35 nm) as compared to CCD (60 and 90 nm). The spectral width also influences magnitude of atmospheric correction on surface reflectances and NDVI. The increase in bandwidth in the red and NIR spectral regions generally tends to decrease NDVI, with most of the changes attributed to the bandwidth difference of the red region[27] only. According to them, for an optimum NDVI definition, the red spectral band should be as narrow as signal-to-noise-ratio consideration that allows less than 50 nm bandwidth for red. Like CCD, even the TM (66 nm) and SPOT HRV (64 nm) sensors have sub-optimum bandwidths in red as compared to MODIS (50 nm).

The view zenith angle played a crucial role on changes of surface reflectance due to surface anisotropy[28]. To study the role of view zenith angle on NDVI datasets, the *in situ* spectroradiometer measurements over an agricultural target were used as shown in Figure 6. The NDVI computed with CCD and MODIS TERRA bandwidths using spectroradiometer measurements showed that the change in view zenith angle showed substantial difference in NDVI between both CCD and MODIS TERRA. Moreover, the MODIS NDVI algorithm considers surface BRDF for NDVI computation whereas in CCD NDVI retrieval, a lambertian surface was assumed. The BRDF is wavelength dependent, and varies with land cover type, consequently the normalizing effect on NDVI does not fully account for the influence of scene geometry[12]. The

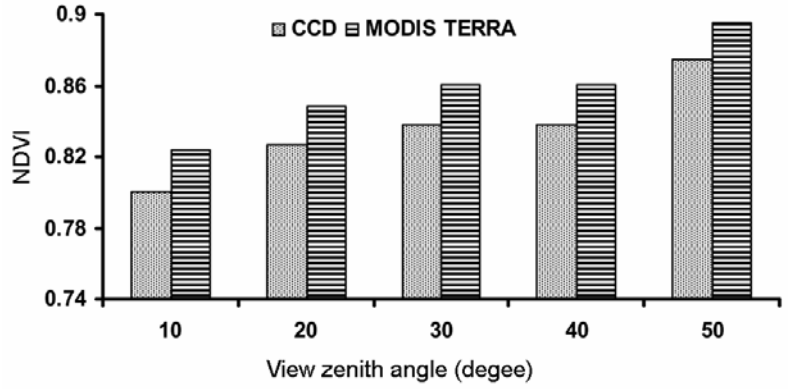

Figure 6. Comparison of NDVI at different view zenith angles for CCD and TERRA spectral bandwidths, and *in situ* spectroradiometer measurements.

BRDF effect is stronger in red region as compared to the NIR region[29].

In the present study, a linear aggregation of MODIS TERRA NDVI from 250 m was applied to scale it up to target the CCD resolution. Different land features such as agricultural fields, urban area, water bodies or natural vegetation patches are often smaller than coarser to moderate resolution pixels[30]. Their varying relative proportion induces sub-pixel heterogeneity. For the native-resolution dataset, the rate of decay is more substantial, i.e. only 26% spatial variability is captured at 250 m spatial resolution of the MODIS dataset and most of the landscape spatial variability is lost at 1 km in both native and aggregated resolution datasets.

Conclusions

A simple correction scheme has been successfully implemented in an operational processing chain to correct TOA reflectance from atmospheric perturbations. This is the first operational vegetation product from Indian geostationary sensor observations over Asia. This product contains surface reflectances in red, NIR, TOA reflectances in SWIR bands, NDVI with cloud flag as well as sun-sensor zenith, azimuth and relative azimuth angles. The operational products are currently available on request from India Meteorological Department (IMD) and are being archived in IMD. The uniqueness of this product is automated generation, low TAT, more assured cloudfree coverage and spatial consistency over the continent. The filling of NDVI data gaps in persistent cloud cover region is still an issue to address vegetation condition or drought during Indian summer monsoon period. Future attempts would be to apply different smoothening and filtering techniques with time series data to obtain temporally consistent NDVI. The characterization of surface BRDF through diurnality of surface reflectances is one of the major future directions of research to improve NDVI product accuracy.

1. Tucker, C. J., Justice, C. O. and Prince, S. D., Monitoring the grasslands of the Sahel 1984–1985. *Int. J. Remote Sens.*, 1986, **7**, 1571.
2. Sellers, P. J., Canopy reflectance, photosynthesis and transpiration. *Int. J. Remote Sens*., 1985, **6**, 1355–1372.
3. Houborg, R., Soegaard, H. and Boegh, E., Combining vegetation index and model inversion methods for the extraction of key vegetation biophysical parameters using Terra and Aqua MODIS reflectance data. *Remote Sens. Environ*., 2007, **106**, 39–58.
4. Xiao, Z., Liang, S., Wang, J., Jiang, B. and Li, X., Real-time retrieval of leaf area Index from MODIS time series data. *Remote Sens. Environ*., 2011, **115**, 97–106.
5. Wardlow, B. D., Egbert, S. L. and Kastens, J. H., Analysis of time-series MODIS 250 m vegetation index data for crop classification in the US Central Great Plains. *Remote Sens. Environ*., 2007, **108**, 290–310.
6. Wardlow, B. D. and Egbert, S. L., Large-area crop mapping using time-series MODIS 250 m NDVI data: an assessment for the US Central Great Plains. *Remote Sens. Environ*., 2008, **112**, 1096–1116.
7. Funk, C. and Budde, M. E., Phenologically-tuned MODIS NDVI-based production anomaly estimates for Zimbabwe. *Remote Sens. Environ*., 2009, **113**, 115–125.
8. Beck, P. S. A., Atzberger, C., Hogda, K. A., Johansen, B. and Skidmore, A. K., Improved monitoring of vegetation dynamics at very high latitudes: a new method using MODIS NDVI. *Remote Sens. Environ*., 2006, **100**, 321–334.
9. Batista, G. T., Shimabukuro, Y. E. and Lawrence, W. T., The long-term monitoring of vegetation cover in the Amazonian region of northern Brazil using NOAA-AVHRR data. *Int. J. Remote Sens*., 1997, **18**, 3195–3210.
10. Wang, Q., Adiku, S., Tenhunen, J. and Granier, A., On the relationship of NDVI with leaf area index in a deciduous forest site. *Remote Sens. Environ*., 2005, **94**, 244–255.
11. Jarlan, L., Mangiarotti, S., Mougin, E., Mazzega, P., Hiernaux, P. and Dantec, V. L., Assimilation of SPOT/VEGETATION NDVI data into a sahelian vegetation dynamics model. *Remote Sens. Environ*., 2008, **112**, 1381–1394.
12. Fensholt, R., Sandholt, I., Stisen, S. and Tucker, C., Analysing NDVI for the African continent using the geostationary meteosat second generation SEVRI sensor. *Remote Sens. Environ.*, 2006, **101**, 212–229.
13. Bhattacharya, B. K., Nigam, R., Dorjee, N., Patel, N. K. and Panigrahy, S., Normalized difference vegetation index-towards development of operational product from INSAT 3A CCD. National Symposium ISRS, 18–20 December 2008.

14. Rao, C. R., Chen, J., Sullivian, J. T. and Zhang, N., Post-launch calibration of meteorological satellite sensors. *Adv. Space Res*., 1999, **23**, 1357–1365.
15. Koagn, F. N., Sullivian, J. T. and Ciren, P. B., Testing post-launch calibration for the AVHRR sensor on world desert targets during 1985–1993. *Adv. Space Res*., 1996, **47**, 47–50.
16. Brest, C. L., Rossow, W. B. and Roiter, M. D., Update of radiance calibrations for ISCCP. *J. Atmos. Ocean. Technol.*, 1997, **14**, 1091–1109.
17. Teillet, P. M. *et al*., A generalized approach to the vicarious calibration of multiple earth observation sensors using hyperspectral data. *Remote Sens. Environ.*, 2001, **77**, 307–327.
18. Eva, H. and Lambin, E. F., Burnt area mapping in central Africa using ASTER data. *Int. J. Remote Sens*., 1998, **19**, 3437–3497.
19. Pandya, M. R., Singh, R. P., Murali, K. R., Babu, P. N., Kirankumar, A. S. and Dadwal, V. K., Bandpass solar exoatmospheric irradiance and Rayleigh optical thickness for Indian remote sensing satellite sensors onboard IRS-1A, 1B, 1C, 1D and P4. *IEEE Trans. Geosci. Remote Sens*., 2002, **40**, 714–718.
20. Rahman, H. and Dedieu, G., SMAC: a simplified method for the atmospheric correction of satellite measurements in the solar spectrum. *Int. J. Remote Sens*., 1994, **15**, 123–143.
21. Gatebe, C. K., King, M. D., Platnick, S., Arnold, G. T., Vermote, E. F. and Schmid, B., Airborne spectral measurements of surface–atmosphere anisotropy for several surfaces and ecosystems over southern Africa. *J. Geophys. Res*., 2003, **108**, 8489, doi:10.1029/2002JD002397.
22. Li, Z., Li, J., Manzel, W. P., Schmit, T. J. and Ackerman, S. A., Comparison between current and future environmental satellite imagers on cloud classification using MODIS. *Remote Sens. Environ*., 2007, **108**, 311–326.
23. Gallo, K., Lei, J., Reed, B., Eidenshink, J. and Dwyer, J., Multiplatform comparisons of MODIS and AVHRR normalized difference vegetation index data. *Remote Sens. Environ*., 2005, **99**, 221–231.
24. Gitelson, A. and Kaufman, Y., MODIS NDVI optimization to fit the AVHRR data series-spectral consideration. *Remote Sens. Environ*., 1998, **66**, 343–350.
25. Miura, T., Yoshioka, H., Fujiwara, K. and Yamamoto, H., Intercomparison of ASTER and MODIS surface reflectance and vegetation index products for synergistic applications to natural recourse monitoring. *Sensors*, 2008, **8**, 2480–2499.
26. Guyot, G. and Gu, X. F., Effect of radiometric corrections on NDVI determined from SPOT HRV and Landsat TM data. *Remote Sens. Environ.*, 1994, **49**, 169–180.
27. Teillet, P. M., Staenz, K. and Williams, D. J., Effect of spectral, spatial, and radiometric characteristics on remote sensing vegetation indices of forested region. *Remote Sens. Environ*., 1997, **61**, 139–149.
28. Steven, M. D., The sensitivity of the OSAVI vegetation index to observational parameters. *Remote Sens. Environ*., 1998, **63**, 49–60.
29. Huete, A. R., Hua, G., Qi, J., Chehbouni, A. and van Leeuwen, W. J. D., Normalization of multidirectional red and NIR reflectance with the SAVI. *Remote Sens. Environ*., 1992, **41**, 143–154.
30. Garrigues, S., Allard, D. and Baret, F., Influence of the spatial heterogeneity on the non-linear estimation of leaf area index from moderate resolution remote sensing data. *Remote Sens. Environ*., 2006, **106**, 286–298.

ACKNOWLEDGEMENTS. We thank Meteorological and Oceanographic Satellite Data Archival Centre for providing the time series INSAT 3A CCD data. We thank Dr R. R. Navalgund, Director, Space Applications Centre, Ahmedabad for his encouragement and support throughout this study. We also thank Shri A. S. Kiran Kumar, Associate Director, SAC and Dr J. S. Parihar, Deputy Director, SAC for their critical suggestions during this study. We are grateful to Dr Sushma Panigrahy, Group Director, Agriculture, Forestry and Environment group for her valuable suggestions while carrying out the analysis. We acknowledge the help and co-operation from Dr V. N. Sridhar for providing spectroradiometer measurements. We thank Dr R. Ramakrishnan, Project Director, IMDPS and his team members for their cooperation. Special thanks are due to officials of Satellite Meteorological Division, IMD for providing the necessary datasets.

Received 1 December 2009; revised accepted 14 January 2011